Journal of Power Sources 195 (2010) 5360–5369

Contents lists available at ScienceDirect

Journal of Power Sources

journal homepage: www.elsevier.com/locate/jpowsour

Multi-walled carbon nanotubes functionalized by carboxylic groups: Activation of TiO_2 (anatase) and phosphate olivines ($LiMnPO_4$; $LiFePO_4$) for electrochemical Li-storage

Ladislav Kavan[a,*], Revathi Bacsa[b], Meltem Tunckol[b], Philippe Serp[b], Shaik M. Zakeeruddin[c], Florian Le Formal[c], Marketa Zukalova[a], Michael Graetzel[c]

[a] J. Heyrovský Institute of Physical Chemistry, v.v.i., Academy of Sciences of the Czech Republic, Dolejškova 3, CZ-18223 Prague 8, Czech Republic
[b] Laboratoire de Chimie de Coordination, UPR CNRS 8241, composante ENSIACET, Université de Toulouse UPS-INP-LCC 4, Allée Emile Monso, BP 74233, 31432, Toulouse, France
[c] Laboratoire de Photonique et Interfaces, EPFL, Ecublens, CH-1015 Lausanne, Switzerland

ARTICLE INFO

Article history:
Received 18 November 2009
Received in revised form 9 February 2010
Accepted 6 March 2010
Available online 12 March 2010

Keywords:
Multi-walled carbon nanotubes
Titanium dioxide
Phosphate olivines
Lithium storage

ABSTRACT

Multi-walled carbon nanotubes functionalized by carboxylic groups, exhibit better affinity towards TiO_2 (P90, Degussa) as compared to that of pristine nanotubes. Also the electrochemical performance of TiO_2 is improved by nanotube networking, but the Li-storage capacity of TiO_2 is unchanged. Whereas the composite of TiO_2 with non-functionalized nanotubes demonstrates simple superposition of the behavior of pure components, the composite with functionalized nanotubes shows unique faradaic pseudocapacitance which is specific for this composite only. The surface functionalization of nanotubes enhances charge storage capacity and reversibility of a composite with $LiMnPO_4$ (olivine), but mediates also the electrolyte breakdown at potentials >4.2 V. Whereas the electrochemical activation of $LiMnPO_4$ (olivine) by functionalized nanotubes is quite modest, excellent performance was found for $LiFePO_4$ (olivine) in composite materials containing only 2 wt% of functionalized nanotubes.

© 2010 Elsevier B.V. All rights reserved.

1. Introduction

Carbon nanotubes form conductive composites with inorganic nanocrystals (for recent review see Ref. [1]). Compared to single-wall carbon nanotubes (SWNT) the multi-walled carbon nanotubes (MWNT) are cheaper, mechanically more robust and their electrical conductivity is less affected by chemical functionalization. Composite materials of MWNT with titanium dioxide have been investigated for application in photocatalysis [2–6] including photocatalytic hydrogen generation [7] and dye-sensitized solar cells [8–11]. In these applications, the beneficial role of MWNT is assumed to consist in improved separation of photogenerated charges, but very low MWNT concentrations (<1 wt%) are required to avoid charge recombination with the electrolyte in dye-sensitized solar cells [8–11]. Improved separation of photogenerated electrons/holes was also demonstrated in solar cells based on band-gap excitation of TiO_2 dispersed on SWNT [12]. The electrochemical lithium storage in carbon nanotube/TiO_2 composites has been studied, too [13–17], reflecting the fact that TiO_2 (especially anatase [18–22], TiO_2(B) [18,23–25] and rutile [18,20,26]) belong to the top interesting host structures for lithium insertion. These studies confirmed in unison that the electrochemical activity of the composite TiO_2/nanotubes is improved compared to that of the parent pure TiO_2 [13–17]. Some authors reported on significantly enhanced Li-storage capacity of the TiO_2/MWNT nanocomposite [13,15], but others [14,16,17] did not support this observation.

From the viewpoint of electrochemical lithium storage, the phosphate olivines [27], *viz.* $LiMPO_4$ (M = Fe, Mn) have been extensively studied in the past. They are promising cathode materials for Li-ion batteries due to high safety, low cost and environmental tolerability. However, their poor electrical conductivity is a crucial issue to be addressed [28] either by doping [29] or by surface coating with elemental carbon [30,31]. The conductivity problem is considerably more significant for $LiMnPO_4$ (conductivity of $\approx 10^{-14}$ S cm^{-1} compared to $\approx 10^{-9}$ S cm^{-1} for $LiFePO_4$) [32] but optimization of the synthesis, that is the formation of carbon coating via ball-milling, provided reasonably active materials, too [33,34].

The effect of MWNT on improvement of the performance of $LiFePO_4$ has been reported by several studies in the past [32,35–42]. The synthetic strategies range from simple mixing [32,36,37,40,41], ball-milling [35,42], hydrothermal synthesis [38], in situ formation of MWNT from ferrocene [39] up to a bio-inspired route, that is a gene manipulation, which was used to align $LiFePO_4$ with SWNT [43]. An analogous electrochemical activation of $LiMnPO_4$ in a com-

* Corresponding author. Tel.: +420 2 6605 3975; fax: +420 2 8658 2307.
E-mail address: kavan@jh-inst.cas.cz (L. Kavan).

0378-7753/$ – see front matter © 2010 Elsevier B.V. All rights reserved.
doi:10.1016/j.jpowsour.2010.03.028

Samsung Ex. 1005, Page 1 of 10
Samsung Electronics Co., Ltd., et al. v. Molecular Rebar Design, LLC
IPR2025-00359

posite with MWNT was reported only recently [32]. In this case, the improvement of charging rate and capacity was quite modest [32], and not comparable to that of the optimized materials, fabricated via ball milling with carbon black [33,34].

The surface oxidation of carbon nanotubes by HNO_3 [6,8,10,15,16,32,37,41,44], H_2SO_4/HNO_3 [4] or H_2O_2 [9], producing among other groups also carboxyls, was sometimes mentioned to improve the anchoring of TiO_2 [4,6,8–10,15,16,44] or $LiMPO_4$ [32,37,41]. In the first case, there is a clear analogy with the strong interaction of carboxyl-containing molecules (Ru-bipyridine dyes) with the TiO_2 surface, which is crucial in dye-sensitized solar cells [10]. However, there are also reports that the oxidative functionalization is not necessary for anchoring to TiO_2, because the pristine MWNT behave similarly [15]. The interaction of carboxyls with phosphate olivine surface is less understood, but certainly important, too [45,46]. To the best of our knowledge, there is no systematic study of these contradictory issues, although detailed understanding is desirable of the MWNT functionalization (by surface oxidation forming carboxyls) for optimum attachment of MWNT towards titania or olivine surfaces.

This was the central motivation for the study reported here. A second argument for deeper investigation of these composites is based on our previous experience with a supramolecular assembly of SWNT with carboxyl-containing Ru–bipyridine complex [45–48]. This assembly offers unique electrochemical activation of $LiFePO_4$ called 'nanotube wiring' [45,46]. The advantage of our nanotube wiring consists in the fact, that it keeps the amount of conductive additives in the active electrode material at its natural minimum (≈0.04 wt% of carbon in $LiFePO_4$). This is important for optimization of Li-ion batteries. The reason is that the electrode materials, *viz*. olivines or TiO_2 [21,22] require *ca*. 10–20 wt% of graphitic carbon to be added. However, graphite does not contribute to the faradaic reaction in the cathode, but presents ballast, decreasing the charge (energy) density of the composite electrode in the same proportion. Obviously, simple oxidation of MWNT is an attractive and cheap alternative to our 'nanotube wiring' effect [45,46] for practical Li-ion batteries. Since TiO_2 is a prospective anode material, and $LiMPO_4$ olivines are promising cathode materials, concerted study of the interaction of MWNT with these three selected materials at defined comparable conditions is relevant for the development of high-power Li-ion batteries.

2. Experimental

Multi-walled carbon nanotubes were prepared from ethylene gas by chemical vapor deposition. The synthesis was carried out in a fluidized bed reactor, and Fe nanoparticles supported on alumina served as catalyst. Details on the reactor configuration and preparation of the catalyst can be found elsewhere [49]. The catalyst was removed by boiling with diluted sulfuric acid (50%) at 140 °C for 3 h after which the nanotubes were filtered when hot by a glass frit followed by washing with hot water and drying at 120 °C. The extraction of catalyst was followed by inductively-coupled mass spectrometry (ICP-MS) analysis, which gave the Al content between 200 and 500 ppm for various samples. For oxidative functionalization, 1 g of purified nanotubes was mixed with 50 mL of 65% HNO_3 and refluxed for 3 h at 120 °C under stirring. The nanotubes were filtered on a glass frit, washed with water until the filtrate reached a pH of 6, and dried at 120 °C for 48 h. The non-functionalized blank material is abbreviated MWNT-bl and the material functionalized by oxidation with HNO_3 is coded MWNT-ox. The extent of functionalization was determined by titration with a freshly prepared aqueous solution of NaOH (0.05 M) as in Ref. [50]. The amount of acid groups in the nanotubes was found to be 2.54×10^{-4} mol g^{-1} in MWNT-ox, and close to 0 in MWNT-bl.

Titanium dioxide P90 (from Degussa AG, Germany) powder had a BET (Brunauer–Emmett–Teller) area of 90 m^2 g^{-1} (rutile/anatase mixture with >90% anatase, average anatase particle size 13 nm). The carbon black Ketjenblack EC-600 was purchased from AkzoNobel. According to the manufacturer's specification, it had an electrical resistivity of 0.01–0.1 Ω cm and the BET specific surface area of 1250 m^2 g^{-1}. Another comparative material was medium-functionalized sample, abbreviated MWNT-mox, which was prepared from MWNT-bl by oxidation with 65%-HNO_3 similarly to MWNT-ox (see above). The titration analysis with 0.05 M NaOH gave the amount of acid groups to be 1.14×10^{-4} mol g^{-1} in MWNT-mox. The carbon-free olivines, $LiFePO_4$ and $LiMnPO_4$ were obtained from High Power Lithium, SA, Switzerland. The nitrogen adsorption isotherms indicated the BET surface areas as of 9 m^2 g^{-1} (for $LiFePO_4$) and 35 m^2 g^{-1} (for $LiMnPO_4$). The latter material was prepared *via* the "polyol" route, and consisted of platelets oriented in the *a*–*c* plane of the olivine lattice [33].

Nanotubes were dispersed in water under short sonication in an ultrasonic bath. To this solution a powder material (TiO_2, $LiMnPO_4$ or $LiFePO_4$) was added (in a proportion of 1–10 wt% of nanotubes in the mixture) and stirred overnight. The suspension was subsequently evaporated to dryness. The electrodes were prepared as follows: powder precursor material, either pure or carbon-containing (see above) was mixed with 5 wt% of polyvinylidene fluoride (PVDF) dissolved in N-methyl-2-pyrrolidone. The resulting slurry was diluted with N-methyl-2-pyrrolidone until a consistence of viscous paste, and then doctor-bladed onto F-doped conducting glass (FTO; TEC 15 from Libbey-Owens-Ford 15 Ω sq^{-1}). The film was cut into smaller pieces of 0.8–1 cm^2 active area, and dried at 100 °C in vacuum. Uncovered area at the edge of the FTO support served for making an electrical contact. The film's mass was between ca. 0.2–1 mg cm^{-2}.

SEM images were obtained using FESEM Philips XL30 FEG instrument. Infrared spectra were recorded on a Perkin-Elmer 1710 Fourier transform spectrophotometer (FTIR) using KBr pellets. ATR-FTIR spectra were measured using a FTS 7000 FTIR spectrometer (Digilab, USA). The spectra were accumulated with the diamond anvil ATR accessory, while the sample powder was pressed against the diamond window. Spectra were derived from 64 scans at a resolution of 2 cm^{-1}.

Electrochemical experiments employed an Autolab PGSTAT potentiostat (Ecochemie) controlled by the GPES 4 software. The electrolyte solution was 1 mol L^{-1} $LiPF_6$ in ethylene carbonate + dimethylcarbonate (EC/DMC; 1/1; w). The reference and counter electrodes were from Li-metal, hence all potentials are quoted against the Li/Li^+ reference electrode in this medium. All electrochemical measurements were carried out in a glove box under Ar-atmosphere.

3. Results and discussion

Fig. 1 shows cyclic voltammogram of thin-film electrode from pure non-functionalized nanotubes, MWNT-bl and the functionalized nanotubes, MWNT-ox. The voltammogram of MWNT-bl confirms an almost ideal double-layer charging in a broad window of electrochemical potentials. Therefore, the voltammetric currents scale with the first power of scan rate, ν as it is expected for capacitive charging:

$$I = \frac{dQ}{dt} = C_{dl} \times \frac{dE}{dt} = C_{dl}\nu, \quad (1)$$

Q is the voltammetric charge, $dE/dt = \nu$ is the scan rate and C_{dl} is the double-layer capacitance. Hence, if we divide the experimental currents by the scan rate and the mass of the electroactive material (m, cf. Fig. 1), we can estimate the specific capacitance, C of our nanotube sample. The found values (averaged from sev-

Samsung Ex. 1005, Page 2 of 10
Samsung Electronics Co., Ltd., et al. v. Molecular Rebar Design, LLC
IPR2025-00359

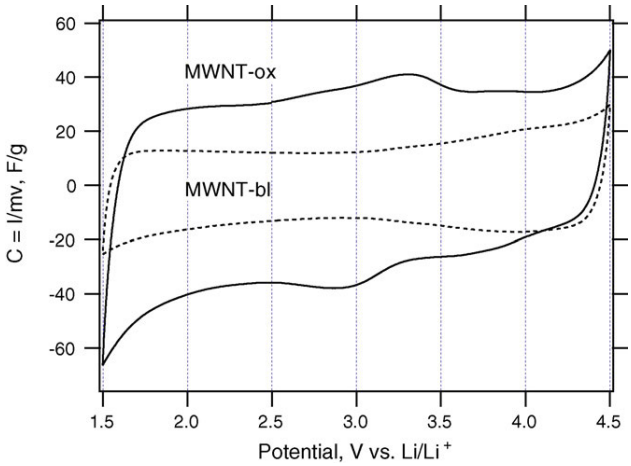

Fig. 1. Cyclic voltammograms of thin film electrodes from pure multi-walled carbon nanotubes, MWNT-bl (dashed curve) and functionalized, MWNT-ox (full curve). Scan rate 0.1 V/s. The current is divided by the scan rate and by the mass of nanotubes in the film, which was 0.26 or 0.22 mg cm^{-2} for MWNT-ox or MWNT-bl, respectively.

eral parallel experiments and varying scan rates) were 12 and 31 F g^{-1} for the MWNT-bl and MWNT-ox, respectively. These capacitances fall among typical values for multi-walled carbon nanotubes in organic electrolyte solutions [51–54]. The MWNT-ox material exhibits characteristic pair of peaks at the formal potential of ca. 3.1 V vs. Li/Li^+. It can be assigned to reversible redox processes in surface oxygen-containing groups [51–56] such as:

$$> C{=}O + e^- \leftrightarrow C{-}O^- \quad (2)$$

which are considered faradaic pseudocapacitance.

The studied materials, *viz.* MWNT-ox and MWNT-bl exhibit significantly different solubility in water and interaction with TiO_2. The first material, MWNT-ox easily dissolves in water to form a black solution, which is stable against flocculation for months at room temperature. Mixing of this solution with TiO_2 (P90) causes immediate blackening of the titania powder and discoloration of the supernatant. In the second case, these effects are not seen: MWNT-bl is insoluble in water and there is only slight coloration of P90 by aqueous suspension of MWNT-bl.

Also the morphology of composites made from these precursors is different. Fig. 2 shows the SEM images of thin film electrodes from TiO_2 (P90), MWNT-ox and the composites TiO_2/MWNT-bl and TiO_2/MWNT-ox; in both cases the concentration of nanotubes is 10 wt%. For the MWNT-ox (right bottom chart), the interaction of nanotubes with titania is excellent. All nanotubes are covered with individual nanocrystals of P90 in a homogeneous nanocomposite. On the other hand, MWNT-bl makes a cracked structure, in which P90 is heavily agglomerated into micron-sized particles, and many 'naked' nanotubes are seen in-between the agglomerates. This morphology is similar to that reported by Tumcharen et al. [11] for pristine multi-walled nanotubes. Presumably, MWNT-bl interact with TiO_2 through small number of defects, and the naked parts of nanotubes are hydrophobic, defect-free areas on the MWNT-bl surface. Obviously, and in contrast to the work of Zeng et al. [15] our data on nanotubes/TiO_2(P90) support the

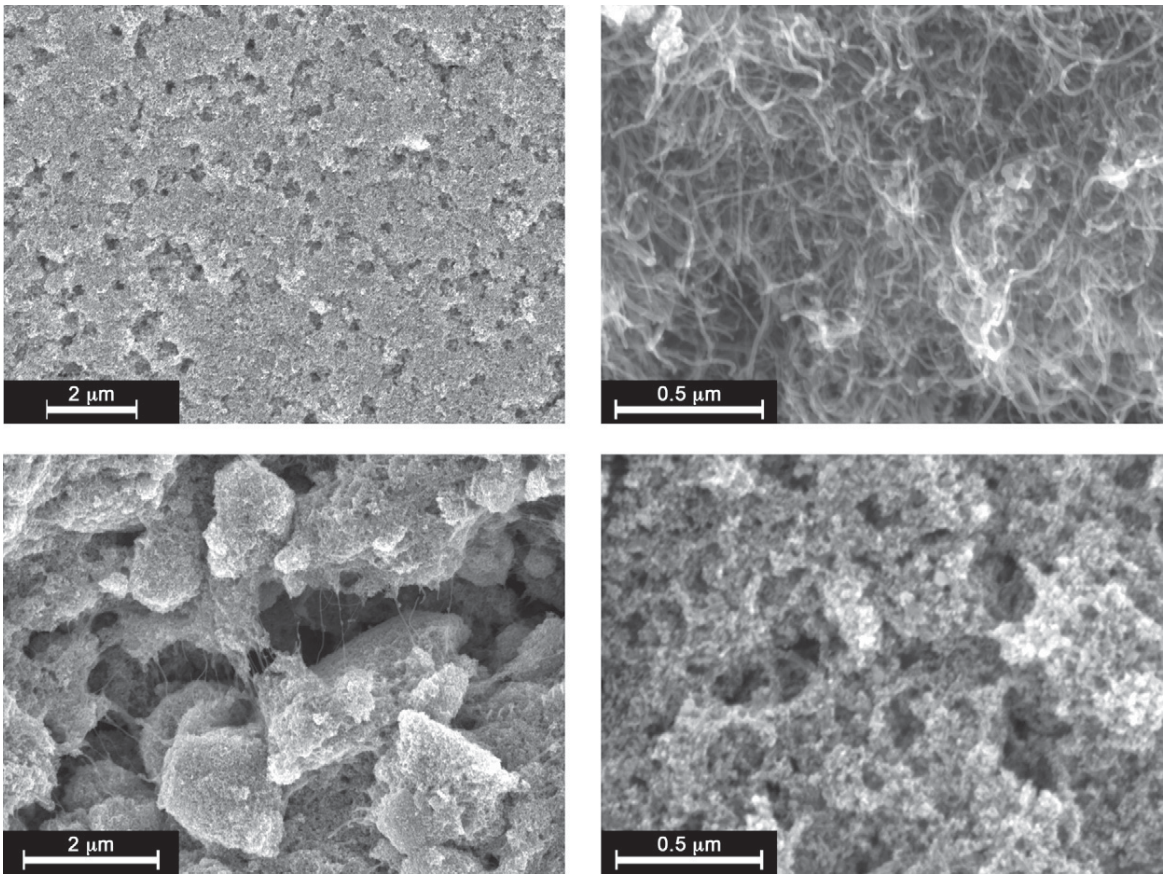

Fig. 2. Scanning electron microscopy images of thin film electrodes from P90 titanium dioxide. (Top left) Pure P90, scale bar 2 μm. (Top right) pure functionalized nanotubes MWNT-ox, scale bar 0.5 μm. (Bottom left) P90 in a composite with 10 wt% of non-functionalized nanotubes MWNT-bl, scale bar 2 μm. (Bottom right) P90 in a composite with 10 wt% of functionalized MWNT-ox, scale bar 0.5 μm.

Samsung Ex. 1005, Page 3 of 10
Samsung Electronics Co., Ltd., et al. v. Molecular Rebar Design, LLC
IPR2025-00359

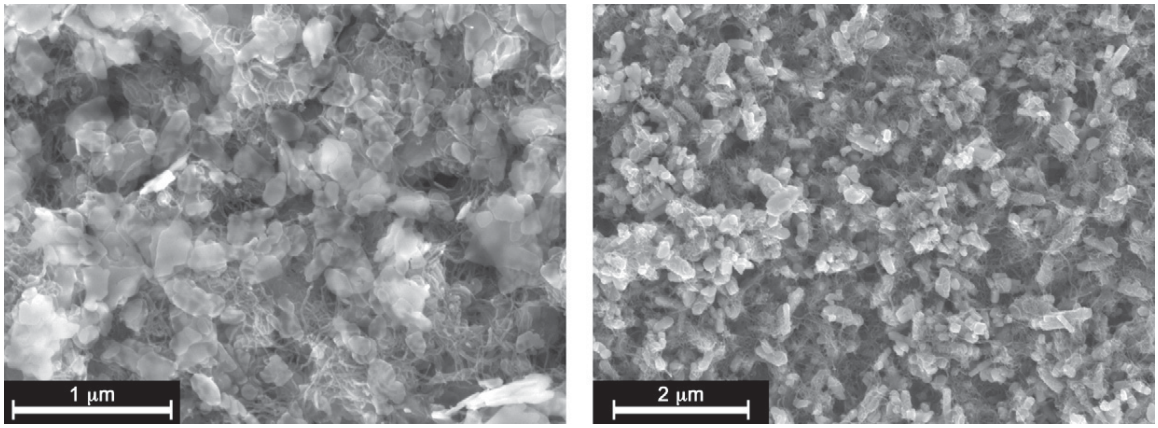

Fig. 3. Scanning electron microscopy images of thin film electrodes from phosphate olivines in a composite with 10 wt% of functionalized nanotubes, MWNT-ox. (Left) Composite with $LiMnPO_4$, scale bar 1 μm. (Right) Composite with $LiFePO_4$ scale bar 2 μm.

idea that oxidative functionalization through HNO_3 is crucial for proper anchoring of nanotubes towards TiO_2. The second message of Fig. 2 is that industrial powder (P90) is a good source of nanocrystals which spontaneously self-assemble on the nanotube surface. This information is important, because previous studies related to nanoparticles grown by laboratory protocols [2–10,13–17].

Fig. 3 shows the morphological features of our olivine/MWNT-ox composites (10 wt% MWNT-ox). In contrast to the structure of P90/MWNT-ox (Fig. 2) the naked nanotubes are easily recognized between the individual crystals of $LiMnPO_4$ (Fig. 3, left chart) as well as between $LiFePO_4$ crystals (Fig. 3, right chart). Two reasons might account for this difference. First, the olivine crystals are typically hundreds of nm in size, whereas the P90 crystals are ca. 10 nm in size. Hence, self-assembling of 10 nm sized crystals on the nanotube, having diameter of ca. 10 nm is feasible, but this kind of packing is hardly achievable with larger crystals. Second, the interaction of –COOH with phosphate surface might be less efficient, than the interaction of carboxyls with titania [10].

Fig. 4 (left panel) shows the FTIR spectra of MWNT-bl and MWNT-ox in KBr pellets. MWNT-ox exhibits the presence of a new band at 1710 cm^{-1} that is attributed to the C=O vibration of the carboxylic groups introduced by oxidative functionalization. The other intense IR band at 1570 cm^{-1} is attributed to the skeletal in-plane vibration of multi-walled nanotube. While MWNT-bl was almost free from surface carboxyls, the sample MWNT-ox contained 2.54×10^{-4} mol g^{-1} acidic groups as determined by titration analysis (see Section 2). The amount of atomic oxygen present on the MWNT-ox surface was also analyzed by X-ray photoelectron spectroscopy (data not shown) that gave a value of 7%. These results are in accordance with those reported earlier for functionalized carbon nanotubes [50]. The sample MWNT-bl further exhibits strong absorption features between 900 and 1300 cm^{-1} with a broad peak at 1110 cm^{-1}. These absorption bands presumably arise from aluminum sulfate impurity in the sample [57] which is introduced during the removal of alumina-supported catalyst by sulfuric acid treatment. The ICP-MS analysis gave the residual concentration of aluminum sulfate in MWNT-bl to be less than 500 ppm (see Section 2). The impurity peaks are not observed in the sample MWNT-ox, hence, they disappear as a result of nitric acid treatment and subsequent washing. In the region around 1200 cm^{-1}, we can also assume the presence of some weak IR bands of C–O and C–C stretching vibrations [57,58]. Although the carbon skeleton can decay and change its vibrational structure as a result of functionalization,

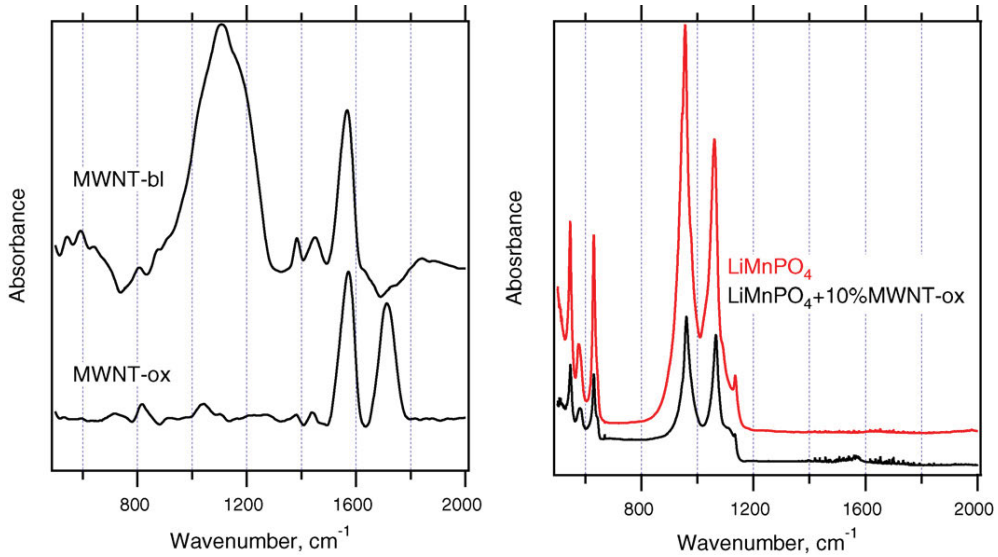

Fig. 4. Left panel: FTIR spectra in KBr pellets of non-functionalized and functionalized nanotubes, MWNT-bl and MWNT-ox, respectively. Right panel: ATR-FTIR spectra of powder of pure $LiMnPO_4$ and $LiMnPO_4$ in a composite with 10 wt% of functionalized nanotubes MWNT-ox. Spectra are offset for clarity.

Samsung Ex. 1005, Page 4 of 10
Samsung Electronics Co., Ltd., et al. v. Molecular Rebar Design, LLC
IPR2025-00359

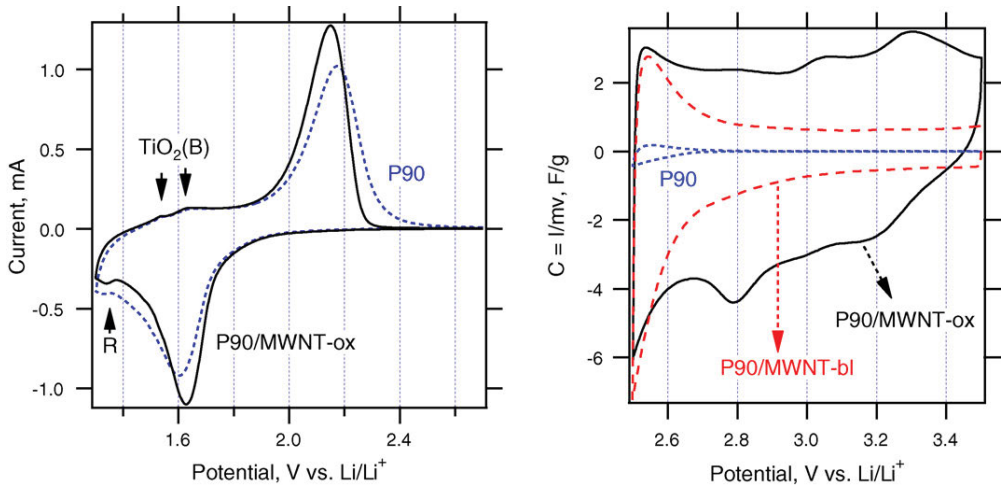

Fig. 5. Cyclic voltammograms of titanium dioxide (P90) thin film electrodes. Full black curves: P90 in a composite with 10 wt% of functionalized nanotubes (P90/MWNT-ox). Dashed blue curve: pure P90. Dashed red curve (right chart only): P90 in a composite with 10 wt% of non- functionalized nanotubes (P90/MWNT-bl). Scan rate 2 mV s^{-1} (left chart) or 50 mV s^{-1} (right chart). The voltammetric features assigned to rutile (R) and TiO_2(B) are marked by arrows. In the right chart, the current is divided by the mass of electrode material and by the scan rate.

there is no conclusive evidence from the IR spectra for this change. First, the skeletal vibration at 1570 cm^{-1} remains intact for both samples and, secondly, the good electrochemical performance of MWNT-ox (see also below) speaks for unperturbed graphitic structure, maintaining high electrical conductivity of nanotubes.

Fig. 4 (right panel) shows ATR-FTIR spectra of the composite $LiMnPO_4$ with 10 wt% MWNT-ox. Also shown is the spectrum of parent pure $LiMnPO_4$. Both spectra are dominated by vibrational features of the PO_4^{3-} group, *viz.* symmetric and antisymmetric bending modes (500–650 cm^{-1}) as well as stretching modes (950–1150 cm^{-1}). These bands remain intact by the interaction with MWNT-ox. The latter component manifests itself by very weak ATR-FTIR features between 1500 and 1800 cm^{-1}, which are assignable to surface oxides including carboxylic groups [50]. These vibration bands are more clearly distinguishable by measurement of MWNT-ox in KBr pellets (left panel, Fig. 4). The vibrational pattern for composites with $LiFePO_4$ is similar (data not shown). Our results are in accord with those for $LiFePO_4$/SWNT/Ru-bipyridine complex, where no shifts of olivine-related vibrations were found upon interaction with nanotubes [47].

Fig. 5 shows the cyclic voltammogram of pure P90 and the composites with nanotubes, P90/MWNT-ox and P90/MWNT-bl. To present comparable data, all electrodes contained similar amounts of TiO_2, around 0.33 mg cm^{-2}. The cyclic voltammograms in the left chart are dominated by a pair of peaks with the formal potential of 1.85 V vs. Li/Li^+, assignable to Li insertion into anatase [18,19,21,22]:

$$x(Li^+ + e^-) + TiO_2 \rightarrow Li_xTiO_2; \quad x \approx 0.5 \tag{3}$$

The total Li-insertion capacity of TiO_2 was determined from the slow scan (0.1 mV s^{-1}) to be 169 or 172 mAh g^{-1} for the P90 or P90/MWNT-ox, respectively. Hence, within the experimental errors, the Li-storage capacities of both materials are identical. This matches the conclusion of most other works on anatase/MWNT composites [14,16,17], although there are also opposite claims for the capacity enhancement in anatase [15]. The beneficial effect of nanotube networking is demonstrated by the shape of cyclic voltammograms of Li-insertion (left chart, Fig. 5): The peak-to-peak separation gets smaller in the composite, and the slopes of insertion onset (around 1.8 V at the cathodic branch) and extraction offset (around 2.2 V at the anodic branch) are steeper for the composite. Particularly, the tail at anodic branch between 2.2 and 2.5 V demonstrates, that extraction of the last portions of the (e^-/Li^+) pairs requires higher overpotential, because the host structure itself (TiO_2) is poorly conducting at these conditions (potentials).

Another important information, which follows from the Li-insertion electrochemistry (Fig. 5, left chart) regards the phase composition of our P90 material. The cathodic peak at 1.35 V is assignable to rutile [18,20,26], which is the expected component of P90 material (see Section 2). Somewhat surprisingly, we also detect tiny amount of monoclinic TiO_2(B) modification of titania. This phase manifests itself by two anodic peaks at 1.55 and 1.65 V, which are diagnostic for the TiO_2(B) phase [25]. It should be noted that the electrochemical Li-insertion is predominantly suitable and highly sensitive method of phase analysis; alternative techniques, viz. X-ray diffraction and Raman spectroscopy did not reveal any TiO_2(B) in our P90 material (data not shown).

Fig. 5 (right chart) shows the details of cyclic voltammogram of our TiO_2–MWNT-ox system in the potential window near the onset of Li-storage in TiO_2. The electrochemical window between 2.5 and 3.5 V is suitable for detailed investigation of pseudocapacitive effects in the composite. Pure TiO_2 expectedly shows no activity, because this potential window is well above the flatband potential, and titania is regarded an insulator in this electrochemical window. The composite TiO_2/MWNT-bl exhibits roughly the capacitive double-layer charging at potentials >ca. 2.8 V, as in pristine MWNT-bl (cf. Fig. 1 and discussion thereof). Because titania is here electrochemically silent, and the concentration of MWNT-bl in the composite was 10 wt%, the found specific capacitance of the composite (≈1 F g^{-1}, cf. Fig. 5, right chart), is assignable solely to that of MWNT-bl.

However, qualitatively new features are observed in the composite TiO_2/MWNT-ox (full curve in Fig. 5, right chart). In contrast to pure MWNT-ox which exhibits just one pair of pseudocapacitive peaks at the formal potential of ca. 3.1 V (Fig. 1), we observe complex pseudocapacitive features in the TiO_2/MWNT-ox composite (Fig. 5, right chart, full curve). A detailed assignment of these peaks cannot be made at this stage, but it is obvious that the interactions between the oxidized (carboxylated) surface of carbon nanotubes and TiO_2 creates new sites for pseudocapacitive interfacial redox chemistry. This matches the conclusion of Reddy and Ramaprabhu [44], but in contrast to this work, we do not observe the dramatic increase of specific capacitance for the composite. The cited authors [44] reported 67 and 160 F g^{-1} for MWNT and TiO_2/MWNT, respectively [44] in aqueous electrolyte solution. Similarly, there was a strong capacitance enhancement in the MWNT composite with

Samsung Ex. 1005, Page 5 of 10
Samsung Electronics Co., Ltd., et al. v. Molecular Rebar Design, LLC
IPR2025-00359

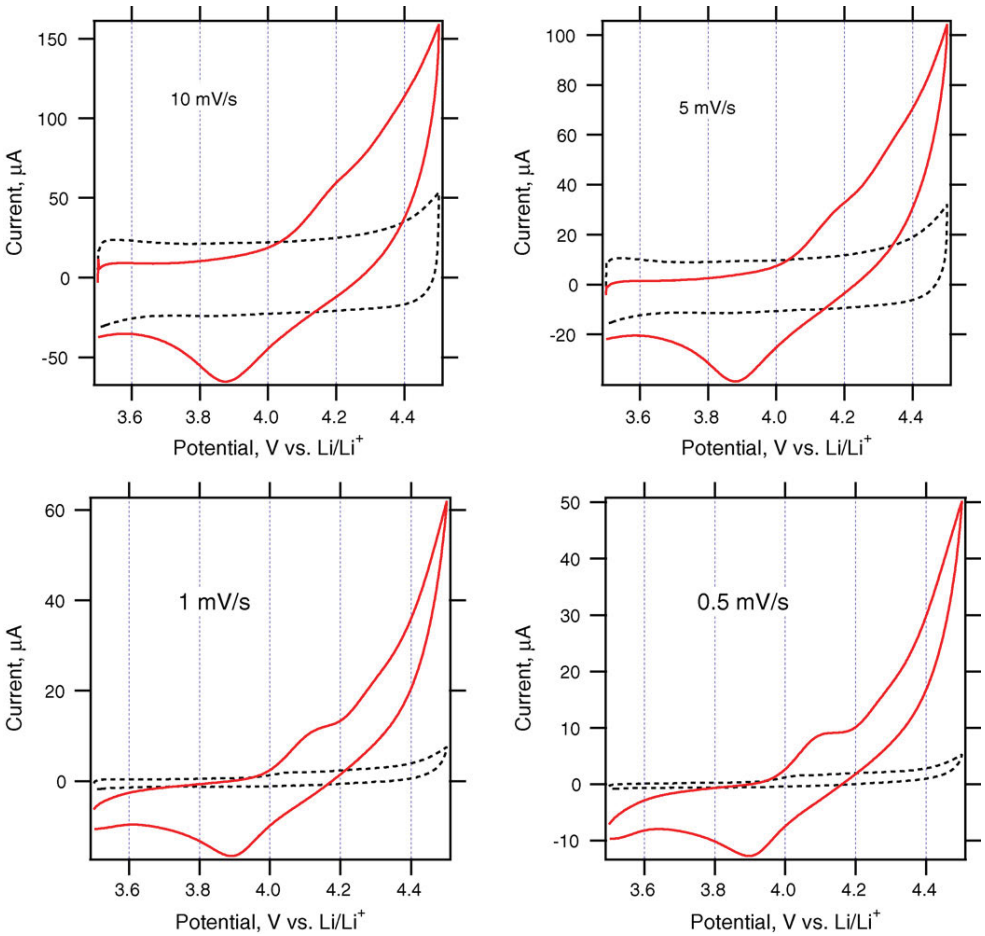

Fig. 6. Cyclic voltammograms of thin film electrodes from $LiMnPO_4$ in a composite with 10 wt% of MWNT-ox (film mass 0.87 mg cm^{-2}; red full curves). The voltammograms of electrodes from pure MWNT-ox are displayed as dashed back curves (film mass 0.20 mg cm^{-2}; these curves are normalized by a factor of 0.435, see text). Scan rates from 10 to 0.5 mV s^{-1} as indicated on each chart.

RuO_2, which is one of the most important oxides for supercapacitors [59]. This was interpreted as coupling of the nanotube-located redox processes (cf. Eq. (2)) with those in protonated ruthenium dioxide:

$$RuO_x(OH)_y + \delta H^+ + \delta e^- \rightarrow RuO_{x-\delta}(OH)_{y+\delta} \quad (4)$$

In our study, employing aprotic Li-containing electrolyte solution, the capacitances are roughly identical (cf. Figs. 1 and 5). Obviously, pseudocapacitive reactions requiring protons are not possible in our electrolyte solution.

Fig. 6 shows a series of cyclic voltammograms of $LiMnPO_4$/MWNT-ox composite (10 wt% MWNT-ox, film mass 0.87 mg cm^{-2}). Also shown are the voltammograms of pure MWNT-ox (the film mass 0.20 mg cm^{-2}; dashed curves in Fig. 6). The latter exhibits just capacitive double-layer charging (cf. Fig. 1). In order to show comparable plots in Fig. 6, the currents for pure MWNT-ox are normalized by a factor of 0.435, which puts the amount of MWNT-ox in both electrodes to identical values. At faster scan rates, we can trace similar voltammetric charge assignable to pure double-layer charging in the composite electrode at potentials around 3.6 V, where no significant faradaic processes in $LiMnPO_4/MnPO_4$ are expected. The latter are found near the formal potential of 4.1 V, which is the Nernstian potential of this reaction [27,33,34]:

$$LiMnPO_4 \leftrightarrow MnPO_4 + Li^+ + e^- \quad (5)$$

The integral cathodic voltammetric charge at the slow scan rate (0.1 mV s^{-1}; data not shown) translates into the reversible charge capacity of 13 mAh g^{-1} at the cut-off voltage of 3.5 V. (The anodic scan provides larger values, which are not representative, because of electrolyte decomposition, see Fig. 6). If we extend the lower cut-off voltage to 3 V, the same electrode provides reversible capacity of 24 mAh g^{-1}. These values are roughly comparable to those of $LiMnPO_4$/MWNT composite reported by Manthiram et al. [32]. They used galvanostatic discharge of an electrode containing 8% of MWNT in $LiMnPO_4$, but their electrodes further contained massive amounts of carbonaceous additives, *viz.* 25 wt% of conductive carbon (of unknown origin) and 25% of teflonized acetylene black [32]. Therefore, their blank electrodes, fabricated from a MWNT-free material, did exhibit discharge capacities of ca. 25–30 mAh g^{-1} (depending on the discharge current) at the cut-off voltage of 2 V, and these values slightly increased to ca. 35–45 mAh g^{-1} for the MWNT-containing material [32].

In our case, the activation of $LiMnPO_4$ by nanotubes is demonstrated on a simpler system, omitting all other carbonaceous additives except MWNT. Fig. 7 confirms that the capacity of pure $LiMnPO_4$ is negligible due to its very low conductivity. Also the beneficial effect of surface oxidation is demonstrated by comparing the composites containing MWNT-bl and MWNT-ox. Here we show the data for nanotube/$LiMnPO_4$ electrodes of roughly comparable film masses around 0.85 mg cm^{-2}. The peak current for anodic process in olivine, that is oxidation of $LiMnPO_4$ to $MnPO_4$ (Eq. (5)) is roughly identical for both electrodes, but the material

Samsung Ex. 1005, Page 6 of 10
Samsung Electronics Co., Ltd., et al. v. Molecular Rebar Design, LLC
IPR2025-00359

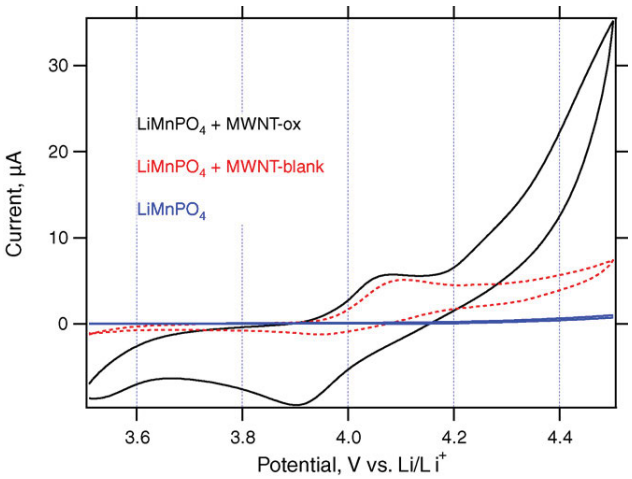

Fig. 7. Cyclic voltammograms of $LiMnPO_4$ thin film electrodes in a composite with 10 wt% of MWNT-ox (film mass 0.83 mg cm^{-2}). Red dashed curve: $LiMnPO_4$ in a composite with 10 wt% of MWNT-bl, film mass 0.87 mg cm^{-2}; the same film like in Fig. 6). Blue curve: pure $LiMnPO_4$ (film mass 1.05 mg cm^{-2}) Scan rate 0.2 mV s^{-1}.

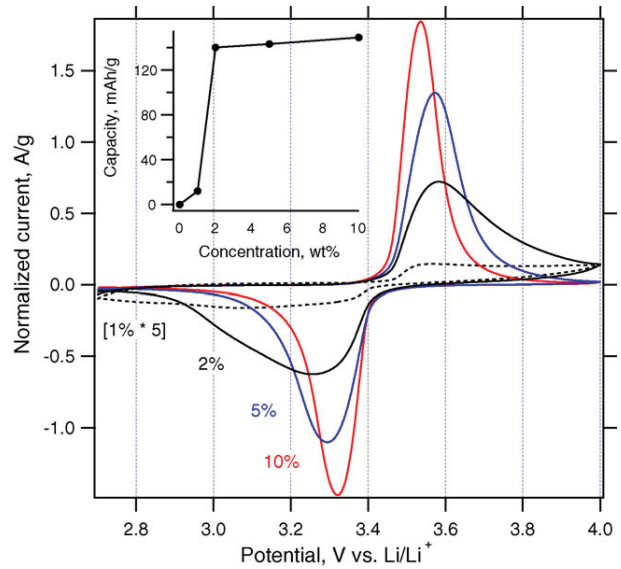

Fig. 9. Cyclic voltammograms of $LiFePO_4$ in a composite with functionalized nanotubes, MWNT-ox. The concentration of MWNT-ox in the composite varied between 1 and 10 wt%. Currents are normalized to the actual mass of $LiFePO_4$ in the thin-film electrode, and for the voltammogram of 1 wt% composite, the current was zoomed by a factor of 5. Scan rate 0.5 mV s^{-1}. Inset shows the integral voltammetric charge capacity as a function of the concentration of MWNT-ox in the composite.

with MWNT-bl shows very small cathodic charge for the reverse reaction. Hence the oxidative treatment of nanotubes improves the reversibility of $LiMnPO_4$ charge/discharge. However, the surface oxidation of nanotubes also activates the electrolyte decomposition. This is demonstrated by anodic branch of our voltammograms between 4.2 and 4.5 V. The surface oxides (carboxyls) mediate these parasitic breakdown reactions, although the mechanism of this activation is unknown. (Note that enhanced breakdown of electrolyte solution is traceable also on pure MWNT-ox film shown in Fig. 1 above.)

In contrast to $LiMnPO_4$ where the electrochemical activation by nanotubes is quite weak, the $LiFePO_4$ olivine exhibits excellent performance in a composite with MWNT-ox. Fig. 8 shows cyclic voltammograms similar to those presented in Fig. 7 for $LiMnPO_4$. The improvement caused by surface oxidation of nanotubes is dramatic. The composite $LiFePO_4$/MWNT-ox exhibits a capacity of 149 mAh g^{-1} (at the scan rate of 0.1 mV s^{-1}) and nearly perfect charge/discharge reversibility of 99–100%. These impressive values were independent on the film mass in the whole tested array of samples, up to ca. 1 mg cm^{-2}. On the other hand, the $LiFePO_4$/MWNT-bl attains only 32 mAh g^{-1} at the same conditions (cf. Fig. 8) although the charging reversibility is again close to 100%. Obviously, the electrolyte breakdown reactions are unimportant for this system, that is charging up to the upper vertex potential of 4 V only, and the charge reversibility is perfect.

This promising system has been subjected to further optimization. Fig. 9 shows cyclic voltammograms for a series of composite materials $LiFePO_4$/MWNT-ox, in which the concentration of MWNT-ox varied. Perfect charge reversibility is again maintained for all materials, but there is a sudden drop of charge capacity for MWNT-ox concentrations between 1 and 2 wt% (see Fig. 9, inset). This seems to be the effective charge-percolation threshold in our composite. Fig. 10 (left chart) further documents this finding by additional performance tests at varying scan rates. The materials with 2–10% MWNT-ox behave roughly similarly, although the performance improves expectedly with increasing concentration. Fig. 10 (right chart) also compares the Li-storage capacity of composite materials with various degrees of nanotube oxidation, that is (in concentrations of acidic groups): 2.54×10^{-4} mol g^{-1}

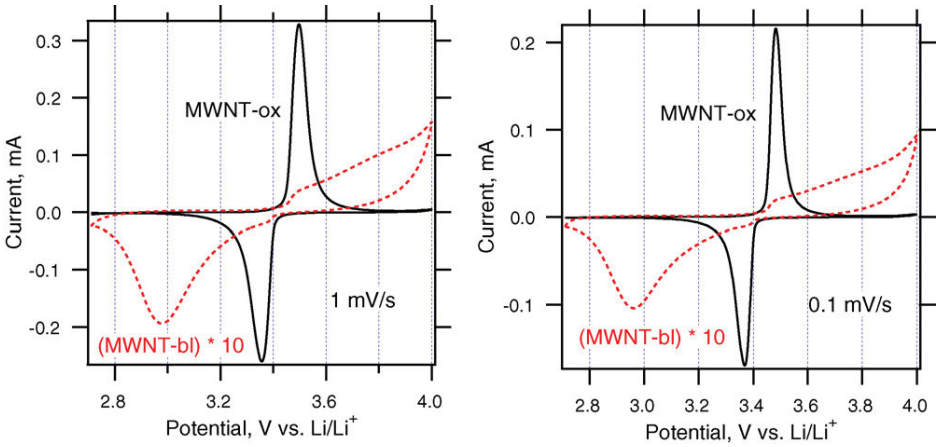

Fig. 8. Cyclic voltammograms of $LiFePO_4$ thin film electrodes. Black full curve: $LiFePO_4$ in a composite with 10 wt% of functionalized nanotubes, MWNT-ox (film mass 0.33 mg cm^{-2}). Red dashed curve: $LiFePO_4$ in a composite with 10 wt% of non-functionalized MWNT-bl (film mass 0.38 mg cm^{-2}); this curve is zoomed by a factor of 10 in the current scale. Scan rate 1 or 0.1 mV s^{-1} for the left or right charts, respectively.

Samsung Ex. 1005, Page 7 of 10
Samsung Electronics Co., Ltd., et al. v. Molecular Rebar Design, LLC
IPR2025-00359

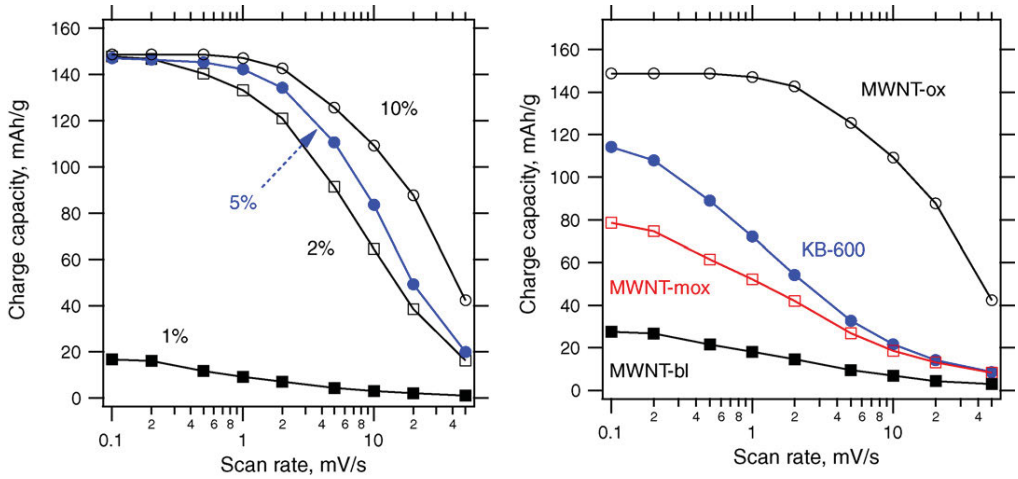

Fig. 10. Integral voltammetric charge capacity as a function of scan rate. (Left chart): $LiFePO_4$ in a composite with functionalized nanotubes, MWNT-ox. The concentration of MWNT-ox in the composite varied between 1 and 10 wt% (as in Fig. 9). (Right chart): $LiFePO_4$ in a composite with the following carbonaceous materials: oxidized nanotubes (MWNT-ox; 2.54×10^{-4} mol g^{-1} acidic groups), medium-functionalized nanotubes (MWNT-mox; 1.14×10^{-4} mol g^{-1} acidic groups), non-functionalized nanotubes (MWNT-bl) and carbon black KB-600. The concentration was 10 wt% in all composites shown in the left chart.

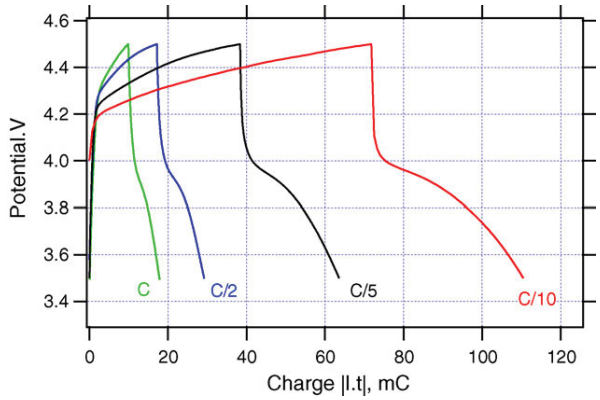

Fig. 11. Galvanostatic chronopotentiometry of $LiMnPO_4$ in a composite with 10 wt% of functionalized nanotubes, MWNT-ox (film mass 0.62 mg cm^{-2}). Discharge/charge cycles are shown for varying charge rates from C/10 to C.

(MWNT-ox); 1.14×10^{-4} mol g^{-1} (MWNT-mox) and ≈0 (MWNT-bl). Somewhat surprisingly, the composite containing MWNT-bl is even less efficient than the composite made from ordinary commercial carbon black, KB-600. It is obvious that the functionalization of nanotubes is, indeed, crucial for enhancing the electrochemical activity of the composite materials with $LiFePO_4$.

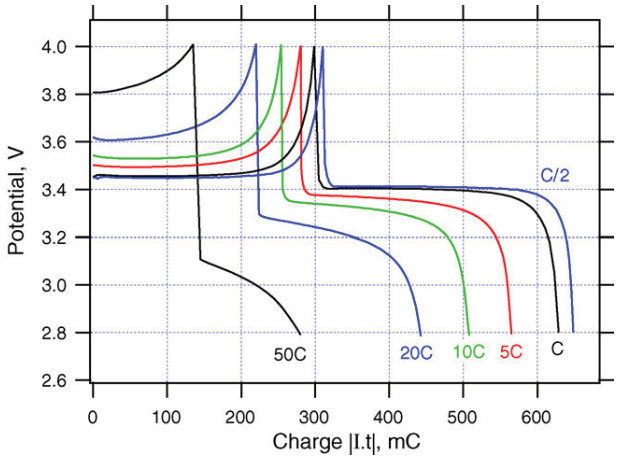

Fig. 12. Galvanostatic chronopotentiometry of $LiFePO_4$ in a composite with 10 wt% of functionalized nanotubes, MWNT-ox (film mass 0.68 mg cm^{-2}). Discharge/charge cycles are shown for varying charge rates from C/2 to 50C.

The conclusions from cyclic voltammetry are further supported by discharge/charge cycles which were tested using galvanostatic chronopotentiometry. Fig. 11 shows the initial discharge/charge of $LiMnPO_4$/MWNT-ox at varying charge rates from C/10 to C. A similar plot for $LiFePO_4$/MWNT-ox is shown in Fig. 12. While the first system exhibits poor performance with considerable irreversibility, the latter is good. The particular electrode shown in Fig. 12 has the theoretical charge capacity of 353 mC (170 mA g^{-1}), while 88% of this capacity can be reversibly cycled at C/2. This electrode can still deliver 38% of its theoretical capacity at 50C, that is within 72 s (Fig. 12). It is interesting to note that the charge capacity observed at C/2, C, 5C, 10C, etc., is roughly similar to the voltammetric charge capacity at scan rates (in mV s^{-1}) of 0.5, 1, 5, 10, etc.

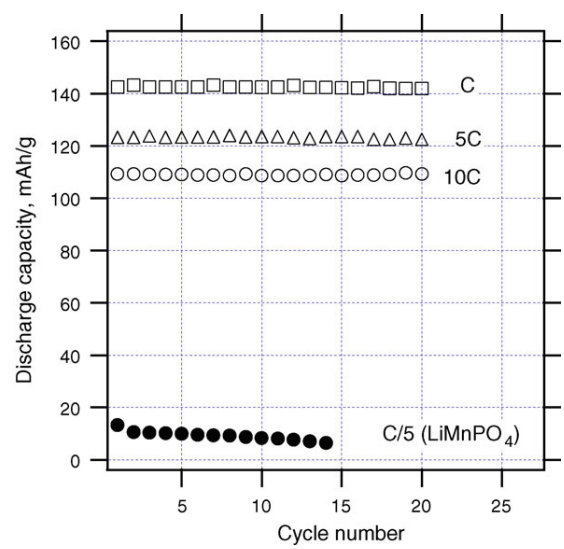

Fig. 13. Discharge capacity determined from galvanostatic chronopotentiometry (as in Figs. 11 and 12) for several successive discharge/charge cycles. The top three curves are for $LiFePO_4$ in a composite with 10 wt% of functionalized nanotubes, MWNT-ox (film mass 0.68 mg cm^{-2}); the charge/discharge rates were: C (squares), 5C (triangles) and 10C (open points). The bottom curve is for $LiMnPO_4$ in a composite with 10 wt% of functionalized nanotubes, MWNT-ox (film mass 0.62 mg cm^{-2}); the charge/discharge rate was C/5 (full points).

Samsung Ex. 1005, Page 8 of 10
Samsung Electronics Co., Ltd., et al. v. Molecular Rebar Design, LLC
IPR2025-00359

(cf. Fig. 10). Obviously, both experiments require comparable times for completing the discharge/charge, and they give similar charge capacities. Fig. 13 shows that the electrode $LiMnPO_4$/MWNT-ox loses ca. half of its initial capacity during 15 subsequent discharge/charge cycles at C/5. This illustrates the conclusions from chronopotentiometry (Fig. 11) and voltammetry (Figs. 6 and 7) that the process is irreversible due to anodic electrolyte breakdown enhanced by MWNT-ox. On the other hand, the cycle life of $LiFePO_4$/MWNT-ox is excellent: we do not see any breakdown during twenty cycles which were repeatedly carried out for the same electrode at C, 5C and 10C (Fig. 13). In subsequent experiments (data not shown) our electrode survived hundreds of cycles without marked decomposition, which would cause any loss of its charge capacity.

4. Conclusions

A comparative study was carried out to investigate composite materials in which multi-walled carbon nanotubes, either pristine or functionalized by carboxyls, were interfaced to three different materials, viz. TiO_2, $LiMnPO_4$ and $LiFePO_4$. The functionalization of nanotubes was followed by FTIR, and by titration analysis of the acidic groups. At comparable conditions, specific features of each combination of materials in the composites are highlighted by electrochemistry in Li-containing aprotic medium.

Functionalized multi-walled carbon nanotubes exhibit improved affinity towards TiO_2. This was demonstrated using industrial powder P90 from Degussa, which is anatase-rutile mixture (>90% anatase) with small amount of TiO_2(B). The latter phase is detectable only by highly sensitive electrochemical analysis shown here. The Li-storage capacity of TiO_2 is not enhanced in the composite, but the rate of electrochemical charge transfer is higher due to nanotube networking. Complex pseudocapacitive features are observed at potentials near the onset of Li-storage in pure anatase. Whereas the composite with pristine nanotubes shows just simple superposition of the behavior of pure components, that is TiO_2 and MWNT-bl (with dominating double-layer capacitive response of pristine MWNT-bl), the composite with functionalized nanotubes shows unique faradaic pseudocapacitance, which is specific only for the interaction of functionalized MWNT-ox with the titania surface.

The composite of $LiMnPO_4$ (olivine) with functionalized multi-walled carbon nanotubes shows enhanced electrochemical charge/discharge performance, which, however, is not comparable to that of the state-of-art carbon-coated $LiMnPO_4$ (olivine). The beneficial effect of surface functionalization consists in improved charge storage capacity and improved charging/discharging reversibility. However, the surface functionalization also promotes the electrolyte breakdown at potentials >4.2 V, which are near the operational conditions of this cathode material in Li-ion batteries.

In contrast to $LiMnPO_4$, excellent electrochemical activation of $LiFePO_4$ by functionalized nanotubes was found. The charging was reversible near 100% and was unperturbed during repeated discharge/charge cycling. This confirms that there was no significant nanotube-mediated electrolyte breakdown at the operating voltage of $LiFePO_4$ (olivine) cathode in Li-ion batteries. Composite material containing only 2 wt% of MWNT-ox showed nearly the nominal charge capacity at the time-scale of cyclic voltammetry, scan rates <0.2 mV s^{-1}. The percolation threshold for nanotube networking of our $LiFePO_4$ was between 1 and 2 wt% of MWNT-ox in the composite. The functionalization of nanotubes via surface oxidation is crucial for the activation of $LiFePO_4$. The composite with pristine nanotubes showed rather low activity, which is even smaller than that of the composite with high surface area carbon black.

Acknowledgements

This work was supported by the Swiss National Science Foundation, Czech Ministry of Education, Youth and Sports (contract No. LC-510 and OC09048), the COST Action D35, and by the Academy of Sciences of the Czech Republic (contract IAA 400400804, KAN200100801 and KAN100500652). We are grateful to HPL, SA for providing us with olivine samples.

References

[1] X. Peng, J. Chen, J.A. Misewich, S.S. Wong, Chem. Soc. Rev. 38 (2009) 1076–1098.
[2] B. Liu, C. Zeng, Chem. Mater. 20 (2008) 2711–2718.
[3] G. An, W. Ma, Z. Sun, Z. Liu, B. Han, S. Miao, Z. Miao, K. Ding, Carbon 45 (2007) 1795–1801.
[4] B. Gao, Z.C. Chen, G.L. Puma, Appl. Catal. B 89 (2009) 503–509.
[5] L.C. Chen, Y.C. Ho, W.S. Guo, C.M. Huang, T.C. Pan, Electrochim. Acta 54 (2009) 3884–3891.
[6] H. Wang, H.L. Wang, W.F. Jiang, Chemosphere 75 (2009) 1105–1111.
[7] K. Dai, T. Peng, D. Ke, B. Wei, Nanotechnology 20 (2009) 125603–1256036.
[8] C.Y. Yen, Y.F. Lin, S.H. Liao, C.C. Weng, C.C. Huang, Y.H. Hsiao, C.C.M. Ma, M.C. Chang, H. Shao, M.C. Tsai, C.K. Hsieh, C.H. Tsai, F.B. Weng, Nanotechnology 19 (2008) 375305–3753059.
[9] T.Y. Lee, P.S. Alegaonkar, J.B. Yoo, Thin Solid Films 515 (2007) 5131–5135.
[10] S.L. Kim, S.R. Jang, R. Vittal, J. Lee, K.J. Kim, J. Appl. Electrochem. 36 (2006) 1433–1439.
[11] T. Sawatsuk, A. Chindaduang, S.K. Chaiyuth, S. Pratontep, G. Tumcharen, Diamond Rel. Mater. 18 (2009) 524–527.
[12] A. Kongkanand, R.M. Dominguez, P.V. Kamat, Nano Lett 7 (2007) 676–680.
[13] D.H. Lee, J.G. Park, K.J. Choi, H.J. Choi, D.W. Kim, Eur. J. Inorg. Chem. 2008 (2008) 878–882.
[14] O. Frank, M. Kalbac, L. Kavan, M. Zukalova, J. Prochazka, M. Klementova, L. Dunsch, Phys. Stat. Sol. (b) 244 (2007) 4040–4045.
[15] J. Li, S. Tang, L. Lu, C. Zeng, J. Am. Chem. Soc. 129 (2007) 9401–9409.
[16] I. Moriguchi, Y. Shono, H. Yamada, T. Kudo, J. Phys. Chem. B 112 (2008) 14560–14565.
[17] H. Huang, W.K. Zgang, X.P. Gan, C. Wamg, L. Zhang, Mater. Lett. 61 (2007) 296–299.
[18] L. Kavan, Adv. Sci. Technol. 51 (2006) 20–29.
[19] M. Wagemaker, W.J.H. Borghols, F.M. Mulder, J. Am. Chem. Soc. 129 (2007) 4323–4327.
[20] D. Wang, D. Choi, V.V. Viswanathan, Z. Nie, C. Wang, Y. Song, J.G. Zhang, J. Liu, Chem. Mater. 20 (2008) 3435–3442.
[21] S.Y. Huang, L. Kavan, M. Grätzel, I. Exnar, J. Electrochem. Soc. 142 (1995) 142–144.
[22] I. Exnar, L. Kavan, S.Y. Huang, M. Grätzel, J. Power Sources 68 (1997) 720–722.
[23] A.R. Armstrong, G. Armstrong, J. Canales, P.G. Bruce, Angew. Chem. Int. Ed. 43 (2004) 2286–2288.
[24] A.R. Armstrong, G. Armstrong, J. Canales, R. Garcia, P.G. Bruce, Adv. Mater. 17 (2005) 862–865.
[25] M. Zukalova, M. Kalbac, L. Kavan, I. Exnar, M. Grätzel, Chem. Mater. 17 (2005) 1248–1255.
[26] N.A. Milne, M.S. Kazacos, V. Luca, J. Phys. Chem. C 113 (2009), 12995-.
[27] A.K. Padhi, K.S. Nanjundasawamy, J.B. Goodenough, J. Electrochem. Soc. 144 (1997) 1188–1194.
[28] B. Ellis, L.K. Perry, D.H. Ryan, L.F. Nazar, J. Am. Chem. Soc. 128 (2006).
[29] S.Y. Chung, J.T. Bloking, Y.M. Chiang, Nat. Mater. 1 (2002) 123–128.
[30] P.S. Herle, B. Ellis, N. Coombs, L.F. Nazar, Nat. Mater. 3 (2004) 147–152.
[31] N. Meetlong, H.Y.J.S. Huang, S.A. Speakman, W.C. Carter, Y.M. Chiang, Adv. Funct. Mater. 17 (2007) 1115–1123.
[32] A.V. Murugan, T. Muraliganth, P.J. Ferreira, A. Manthiram, Inorg. Chem. 48 (2009) 946–952.
[33] D. Wang, H. Buqa, M. Crouzet, G. Deghenghi, T. Drezen, I. Exnar, N.H. Kwon, J. Miners, L. Poletto, M. Grätzel, J. Power Sources 189 (2009) 624–628.
[34] S.K. Martha, B. Markovsky, J. Grinblat, Y. Gofer, O. Haik, E. Zinigrad, D. Aurbach, T. Drezen, D. Wang, G. Deghenghi, I. Exnar, J. Electrochem. Soc. 156 (2009) A541–A552.
[35] B. Jin, H.B. Gu, W. Zhang, K.H. Park, G. Sun, J. Solid State Electrochem. 12 (2008) 1549–1554.
[36] Y. Liu, X. Li, H. Guo, Z. Wang, W. Peng, Y. Yang, R. Liang, J. Power Sources 184 (2008) 522–526.
[37] X. Li, F. Kang, X. Bai, W. Shen, Electrochem. Commun. 9 (2007) 663–666.
[38] J.C. Chen, M.S. Whittingham, Electrochem. Commun. 8 (2006) 855–858.
[39] M.M. Doeff, J.D. Wilcox, R. Yu, A. Aumentado, M. Marcinek, R. Kostecki, J. Solid State Electrochem. 12 (2008) 995–1001.
[40] L. Wang, Y. Huang, R. Jiang, D. Jia, J. Electrochem. Soc. 154 (2007) A1015–A1019.
[41] T. Muraliganth, A.V. Murugan, A. Manthiram, J. Mater. Chem. 18 (2008) 5661–5668.
[42] B. Jin, K.H. Park, H.B. Gu, Electrochem. Commun. 10 (2008) 1537–1540.
[43] Y.J. Lee, H. Yi, W.J. Kim, K. Kang, D.S. Yun, M.S. Strano, G. Ceder, A.M. Belcher, Science 324 (2009) 1051–1055.
[44] A.L.M. Reddy, S. Ramaprabhu, J. Phys. Chem. C 111 (2007) 7727–7734.
[45] L. Kavan, I. Exnar, J. Cech, M. Grätzel, Chem. Mater. 19 (2007) 4716–4721.

Samsung Ex. 1005, Page 9 of 10
Samsung Electronics Co., Ltd., et al. v. Molecular Rebar Design, LLC
IPR2025-00359

[46] L. Kavan, I. Exnar, S.M. Zakeeruddin, M. Grätzel, J. Phys. Chem. C 112 (2008) 8708–8714.
[47] L. Kavan, S.M. Zakeeruddin, I. Exnar, M. Grätzel, J. Electrochem. Soc. 156 (2009) K44–K50.
[48] L. Kavan, O. Frank, M. Kalbac, L. Dunsch, J. Phys. Chem. C 113 (2009) 2611–2617.
[49] M. Corrias, B. Caussat, A. Ayral, J. Durand, Y. Kihn, P. Kalck, P. Serp, Chem. Eng. Sci. 58 (2003) 4475–4482.
[50] A. Solhy, B.F. Machado, J. Beausoleil, Y. Kihn, F. Goncalves, M.F.R. Pereira, J.J.M. Orfao, J.L. Figueiredo, J.L. Faria, P. Serp, Carbon 46 (2009) 1194–1207.
[51] E. Frackowiak, K. Metenier, V. Bertagna, F. Beguin, Appl. Phys. Lett. 77 (2000) 2421–2423.
[52] C. Li, D. Wang, X. Wang, J. Liang, Carbon 43 (2005) 1557–1583.
[53] E. Frackowiak, S. Gautier, H. Gaucher, S. Bonnamy, F. Béguin, Carbon 37 (1999) 61–69.
[54] E. Frackowiak, F. Béguin, Carbon 40 (2002) 1775–1787.
[55] C.C. Hu, J.H. Su, T.C. Wen, J. Phys. Chem. Solids 68 (2007) 2353–2362.
[56] Y.T. Kim, Y. Ito, K. Tadai, T. Mitani, U.S. Kim, H.S. Kim, B.W. Cho, Appl. Phys. Lett. 87 (2005) 234106–2341063.
[57] J.T. Kloprogge, R.L. Frost, Thermochim. Acta 320 (1998) 245–252.
[58] T.G. Ros, A.J. van Dillen, J.W. Geus, D.C. Konigsberger, Chem. Eur. J. 8 (2002) 1151–1162.
[59] G. Arabal, D. Wang, M. Kulkarni, I.S. Mulla, S.P. Vernekar, K. Vijayamohanan, A.M. Rao, Chem. Phys. Lett. 376 (2003) 207–213.

Samsung Ex. 1005, Page 10 of 10
Samsung Electronics Co., Ltd., et al. v. Molecular Rebar Design, LLC
IPR2025-00359